

Performance of Concrete-Filled FRP Tubes under Field Close-in Blast Loading

Yazan Qasrawi¹; Pat J. Heffernan²; and Amir Fam, M.ASCE³

Abstract: Blasts, whether deliberate or accidental, are a great concern for a society's critical infrastructure as well as expeditionary military installations. Improvement to existing construction methods that enhance blast resilience can ultimately save lives and property. Concrete-filled FRP tubes (CFFT) are known to improve a conventional reinforced concrete member's resistance to traditional loads by strengthening, protecting, and confining the reinforced concrete core. Glass fibre reinforced polymer (GFRP) tubes are readily available in a variety of sizes suitable for use as a stay-in-place structural formwork for midsized reinforced concrete members, which can simplify and expedite construction. These advantages point to CFFT's great potential in resisting blast loads. This study aimed to quantify the advantages of encasing a reinforced concrete member with a GFRP tube subjected to close-in blast loading and to investigate the effects of the presence of the tube, the internal steel reinforcement ratio, and the blast scaled distance on CFFT's behavior under blast loading. This was accomplished by testing four CFFT and reinforced concrete specimen pairs under blast and monotonic loading. The specimens were tested in pairs to facilitate comparisons. The CFFT specimens performed significantly better than the conventional reinforced specimens, showing greater robustness with decreased localized damage and reduced residual displacements. This indicated the need for developing analysis and design procedures for this system. Therefore, a procedure for developing Pressure-Impulse diagrams for the tested CFFT specimens was outlined and their use for the design of CFTTs under close-in blast loads was explained. A numerical procedure for developing equivalent close-in blast forcing functions was also outlined. DOI: [10.1061/\(ASCE\)CC.1943-5614.0000502](https://doi.org/10.1061/(ASCE)CC.1943-5614.0000502). © 2014 American Society of Civil Engineers.

Author keywords: Concrete-filled FRP tube (CFFT); Fibre reinforced polymer (FRP) tube; SDOF model; Close-in blast; Pressure–impulse diagrams.

Introduction

The need to protect civilian, industrial, and military structures from intentional or accidental explosions is of paramount importance to save lives and property. Close-in blasts are the most severe in-air explosions a structure can experience. Their proximity to the structure also makes them the most difficult to predict, analyze, and design against.

Durable and lightweight commercially available GFRP tubes come in a variety of sizes and can be used as stay-in-place structural forms for concrete construction. When used as stay-in-place forms, GFRP tubes confine the concrete core and act as structural reinforcement, which is ideally located at the perimeter to resist axial and flexural loads. These advantages point to the potential of using concrete-filled FRP tubes (CFTTs) in blast resistant design, especially in expeditionary military installations.

CFTTs have already been implemented for bridge piers, marine piles, and girders (Fam and Mandal 2006) and are promising for utility and light pole applications (Qasrawi and Fam 2008). The static performance of CFTTs has been investigated extensively, as in the investigation by Fam and Rizkalla (2002) of the flexural performance of CFTTs, the study by Cole and Fam (2006) of the enhancement of CFTTs by the introduction of internal steel and FRP reinforcement, the study by Fam and Mandal (2006) on pre-stressing the system, and the study of their behavior under combined axial and flexural loads by Flisak et al. (2001). Helmi et al. (2008) investigated the important problem of the fatigue behavior of GFRP tubes, and Elgawady et al. (2010) and Zaghi et al. (2012) investigated the seismic behavior of CFTTs in two separate studies. Although many aspects of the static behavior of CFTTs have been investigated, their behavior under blast loading remained to be investigated.

Fujikura et al. (2008) have observed experimentally and Qasrawi et al. (2010) have demonstrated numerically that blast shockwaves diffract around circular cross sections, imparting less energy to them. This evidence pointed to the advantages to be gained from using a round geometry in blast-resistant construction.

Malvar et al. (2007), Buchan and Chen (2007), and Crawford (2013) examined the use of composites to increase the blast resistance capacity of a variety of structural elements such as reinforced concrete beams, columns, slabs, and walls, as well as masonry walls. Malvar et al. (2007) concluded that composites in the form of wrapping or near-surface mounted plates increased the strength of existing members and helped prevent the collapse of load bearing members that may initiate a progressive collapse of the structure. Buchan and Chen (2007) compared the results of experimental and numerical investigations of the effectiveness of retrofitting structures using FRP. They concluded that FRPs improved a structure's strength and

¹Assistant Professor, Dept. of Civil Engineering, Royal Military College of Canada, P.O. Box 17000, Station Forces, Kingston, ON, Canada K7K 7B4 (corresponding author). E-mail: Yazan.Qasrawi@rmc.ca

²Vice-Principal, Research and Dean of Graduate Studies, Dept. of Civil Engineering, Royal Military College of Canada, P.O. Box 17000, Station Forces, Kingston, ON, Canada K7K 7B4. E-mail: Pat.Heffernan@rmc.ca

³Donald and Sarah Munro Chair in Engineering and Applied Science Professor and Chair of Undergraduate Studies, Dept. of Civil Engineering, Queen's Univ., Kingston, ON, Canada K7L 3N6. E-mail: fam@civil.queensu.ca

Note. This manuscript was submitted on February 23, 2014; approved on June 11, 2014; published online on September 29, 2014. Discussion period open until February 28, 2015; separate discussions must be submitted for individual papers. This paper is part of the *Journal of Composites for Construction*, © ASCE, ISSN 1090-0268/04014067(12)/\$25.00.

stiffness, but that the behavior was not well understood due to the complexity of the problem and that most of the studies provided qualitative rather than quantitative results. They urged the development of design guidelines, which are essential for the widespread use of FRP for blast-resistant applications. They also noted that not reporting some sensitive information made comparisons between studies difficult. Crawford (2013), on the other hand, looked specifically at the use of FRP to enhance the blast resistance of reinforced concrete columns. He concluded that FRP offers great capabilities for column enhancement against blast, especially by increasing flexural capacity and confining the concrete core. Additionally, Crawford (2013) recommended the use of "high fidelity physics-based" finite element techniques for the analysis of highly variable blast scenarios with an emphasis on selecting the concrete material model carefully. These studies stressed that strengthening columns was of particular importance because they tend to be load bearing members whose collapse may initiate the progressive collapse of a structure.

The simplified handling and rapid construction, additional resistance capacity, confinement of the concrete core, and reduced blast loading all suggest that CFFT members have great potential for blast-resistant construction.

This investigation studied the performance of CFTTs under close-in blast loading when compared to concrete members with identical internal steel reinforcement.

The objectives of this study were:

1. To experimentally demonstrate the superiority of CFTTs compared to conventional reinforced concrete members in resisting close-in blast loading;
2. To develop a procedure for obtaining a close-in blast equivalent forcing function using the commercially available software *ANSYS Autodyn*; and
3. To outline a procedure for developing Pressure-Impulse diagrams for use as a design tool for CFTTs.

This paper presents the methodology and results of the testing of eight full-scale CFFT and reinforced concrete specimens monotonically and under close-in blast followed by a discussion of the results. A detailed procedure for developing a close-in blast equivalent forcing function is then presented. Finally, a procedure for developing Pressure-Impulse diagrams for use as a design tool is outlined.

Experimental Program

Materials

The concrete strength of 34 MPa was obtained by performing six cylinder compression tests according to CSA standard A23.2-9C [Canadian Standards Association (CSA) 2004a]. Three tests were also performed on the utilized 6 mm and 10M steel reinforcing bar diameters used to obtain their tensile properties. The 6 mm bars had a yield strength of 645 MPa and an ultimate strength of 713 MPa with a modulus of elasticity of 194 GPa. The 10M bars had a yield strength of 430 MPa, and an ultimate strength of 577 MPa with a modulus of elasticity of 170 GPa. The GFRP tube's mechanical properties were obtained from the manufacturer (Ameron International 1988). The tube had a hoop tensile strength of 128 MPa, a hoop tensile modulus of 21.6 GPa, and a Poisson's ratio of 0.45, as well as a longitudinal tensile strength of 48.3 MPa, and modulus of 10.1 GPa, and a Poisson's ratio of 0.35. The GFRP tubes had an outer diameter of 0.22 m and a structural wall thickness of 5.5 mm. The tubes' walls consisted of continuous glass fibers wound at a $\pm 55^\circ$ helical angle relative to the long axis in a premium vinyl ester resin matrix.

Test Specimens and Parameters

Eight reinforced concrete test specimens were cast in the structures lab of the Royal Military College of Canada (RMC). The specimens were 4 m long and had a circular cross section with a nominal diameter of 0.2 m. Three specimens were cast using conventional commercial cardboard tubes, and three specimens, with identical internal steel reinforcement, were cast using the GFRP tubes as stay-in place formwork. Of the eight specimens, six had a steel reinforcement ratio of 2.4%, in the form of eight-10M longitudinal reinforcing bars, and two had a steel reinforcement ratio of 1.2% in the form of four-10M longitudinal reinforcing bars. The steel reinforcement ratios of 1.2 and 2.4% were selected to reflect the 1% minimum and 2.5% maximum reinforcement ratios recommended for blast resistant design [Unified Facilities Criteria (UFC) 3-340-01 2002; Canadian Standards Association 2004a] to ensure sufficient strength and a ductile failure. All the specimens contained 6-mm-diameter continuous steel spiral reinforcement to prevent shear failure and maximize ductility. The pitch of the spiral was 0.1 m, except over the supports where it was reduced to 0.05 m over a length of 0.2 m from both ends to mitigate the reactions concentrated loading. Fig. 1 provides schematics of the four different cross section configurations for the eight specimens. All the specimens were tested in the orientation shown in the figure. A summary of the test matrix is also presented in Table 1.

Data Acquisition Systems and Instrumentation

Unfortunately, due to technical issues associated with damage due to the close-in blasts, much of the instrumentation discussed in this section did not provide the desired results. Three separate Data Trap II modules, manufactured by MREL collected the blast data: one dedicated to the strain gauge measurements, one dedicated to the pressure probe data, and one collected the LVDT and accelerometer data. The data from the pressure probes, LVDTs, and accelerometers were recorded at 5MHz while the strain gauge data was recorded at the maximum rate of the module of 100 kHz. The instrumentation consisted of four strain gauges on the steel reinforcing bars at midspan per specimen, a high-speed camera, a LVDT, and an accelerometer at midspan per specimen for most tests. Four free-field pressure probes were placed at various distances ranging from 2.5 to 25 m. The locations of the pressure probes were modified based on the charge size. The data acquisition and the recording of the high-speed camera were triggered by the explosion.

Monotonic Testing Setup and Procedure

Specially designed blast testing frames were used to support the specimens during both the blast and the monotonic testing phases. A schematic of the monotonic test set up is shown in Fig. 2. Specimens CM8 and TM8 were tested monotonically in four-point bending. The clear span was 3.85 m and the applied point loads were 0.55 m apart. The tests were carried out under displacement control at a constant stroke rate of 1 mm/min. Steel sleeves 0.15 m long were placed at the supports and under the loading points to distribute the loads and prevent local failure. During testing, the displacement of specimen TM8 exceeded the machine's stroke, therefore, after reaching maximum stroke, it was unloaded and spacers were added before reloading to failure.

Blast Testing Setup and Procedure

Full-scale blast tests were conducted at the Canadian Forces Base in Petawawa, Ontario with the assistance of 2 Combat Engineers Regiment (2 CER). The testing frames were placed side by side to

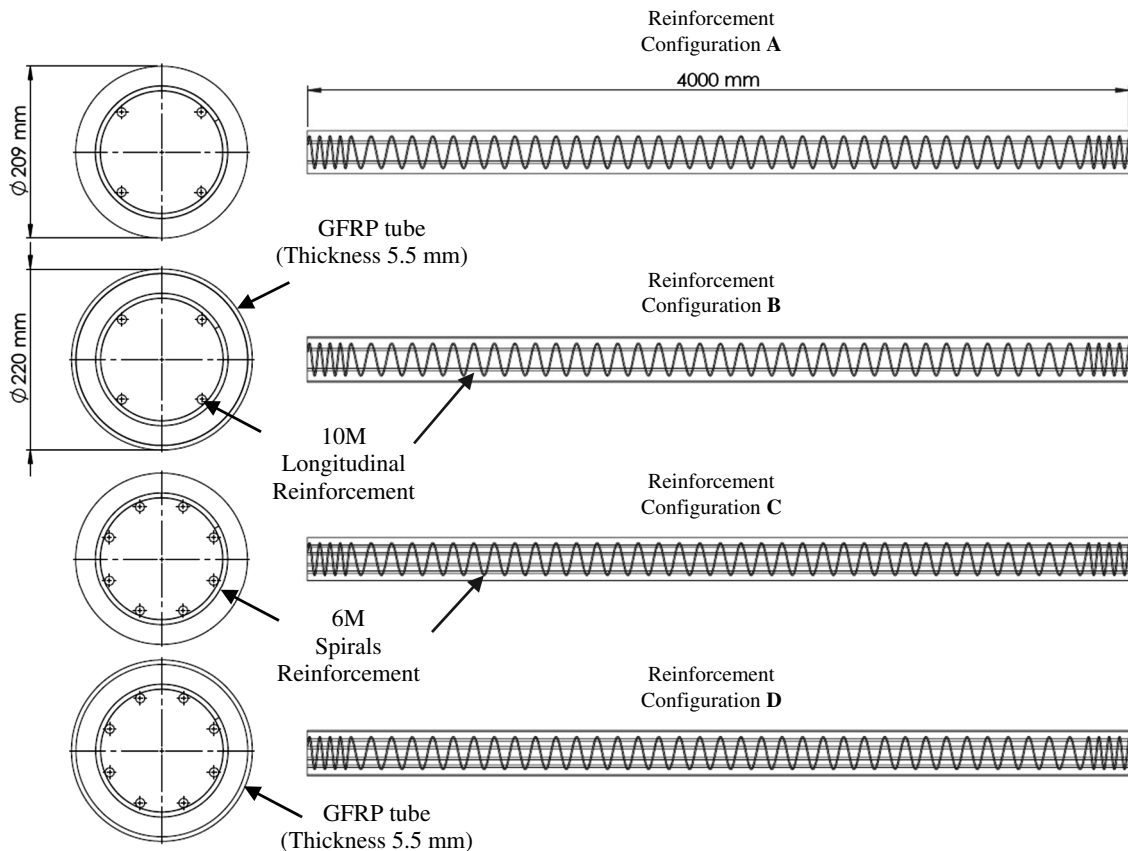


Fig. 1. Specimens' reinforcement configurations

Table 1. Test Matrix

Specimen	Testing method	Type	Reinforcement ratio (%)	Reinforcement configuration
CB4	50 kg C4	RC	1.2	A
TB4	50 kg C4	CFFT	1.2	B
CB8-S	50 kg C4	RC	2.4	C
TB8-S	50 kg C4	CFFT	2.4	D
CB8-L	100 kg C4	RC	2.4	C
TB8-L	100 kg C4	CFFT	2.4	D
CM8	Monotonic	RC	2.4	C
TM8	Monotonic	CFFT	2.4	D

subject the test and control specimens to the same testing conditions. The instrumentation wires were run through ducts incorporated in the slabs for that purpose. Sand bags were used to cover all exposed wires. The LVDTs were placed inside welded steel boxes below the specimens to protect them. Two 0.15-m-long steel sleeves were used at the ends of the specimens to distribute the support loading and prevent local failure.

The spherical explosive charges were supported on wooden frames 2 m above the top face of the specimens. A schematic of this setup is shown in Fig. 3. The first pair of blast specimens, CB8-S and TB8-S, were not damaged by the initial charge of

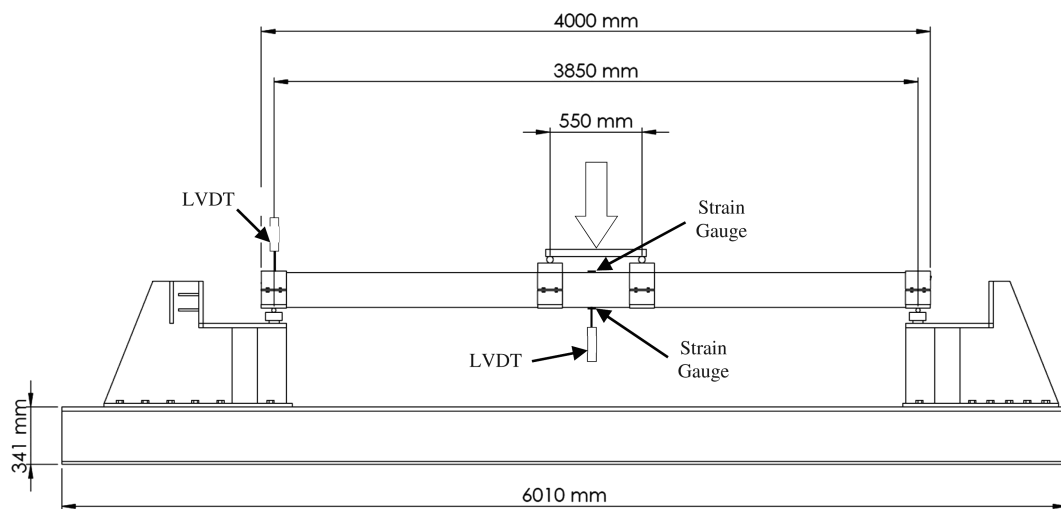


Fig. 2. Schematic of monotonic testing setup

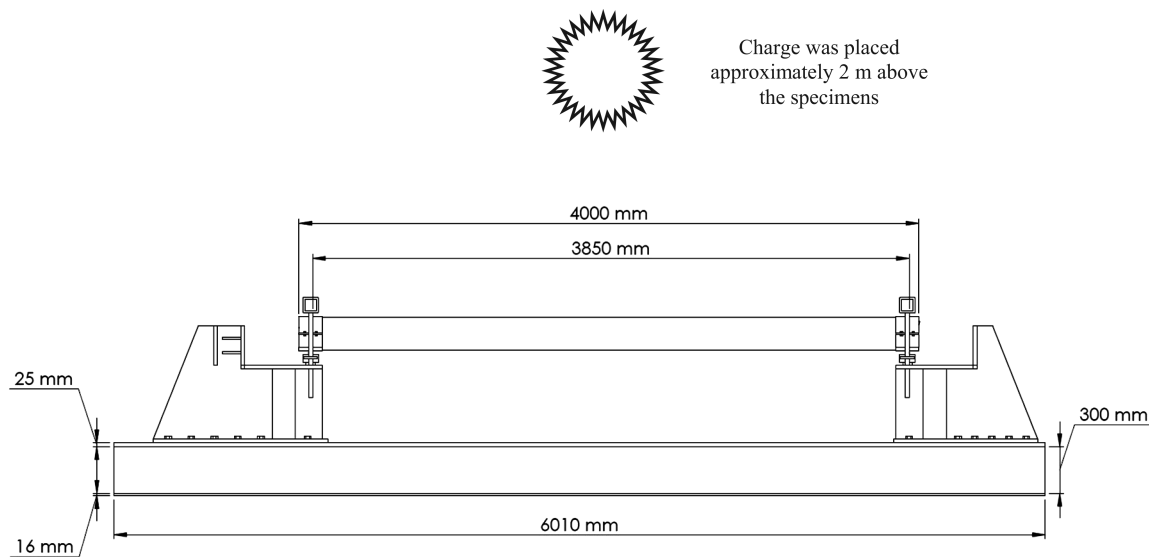


Fig. 3. Schematic of blast testing setup

Table 2. Blast Parameters of Test Charges

Mass C4 (kg)	Equivalent mass TNT (kg)		R (m)	Z ($\text{m} \cdot \text{kg}^{-1/3}$)		P_r (MPa)	I_r (MPa · ms)	P_{so} (MPa)	I_{so} (MPa · ms)
	Pressure	Impulse		Pressure	Impulse				
Blast parameters at midspan									
15	20.55	17.85	2.13	0.78	0.81	10	1.97	1.7	0.42
30	41.1	35.7	2.17	0.63	0.67	16	3.30	2.3	0.59
50	68.5	59.5	2.20	0.54	0.56	25	5.09	3.0	0.59
100	137	119	2.25	0.44	0.46	40	8.88	5.0	0.74
Blast parameters at support									
50	68.5	59.5	2.92	0.71	0.75	12	3.51	2.0	0.71
100	137	119	2.96	0.58	0.61	18	4.92	3.0	0.79

15 kg of C4, therefore, the charge mass was increased incrementally until initial damage was observed. The increments were 15, 30, and 50 kg of C4. Once damage to the specimens was observed, the second pair of blast specimens, CB4 and TB4, was substituted and tested at the same explosive mass to facilitate comparison. Partly because the visible damage to specimens CB8-S and TB8-S was minimal, and partly due to time limitations, the quantity of explosives used for specimens CB8-L and TB8-L was doubled to 100 kg of C4. The blast equivalent TNT mass for the test charges, distance from the centre of the charge to midspan of the specimen, scaled distance, and chart blast parameters are presented in Table 2. Two equivalent TNT masses are presented as the UFC 3-340-01 (UFC 2002) provides different equivalency factors for the equivalent pressure and the equivalent impulse. The scaled distances in Table 2 include the 2 m height of the wooden support frames as well as the radius of the charge to give the distance to the centre of the explosive. To give an indication of the variation in the blast effects over the length of the specimen, Table 2 also includes the scaled distance, reflected, and side-pressure and impulses over the support, accounting for the inclined angle of incidence, for the 50 and 100 kg of C4 charges.

Experimental Results

Loads and Displacements of Monotonic Tests

The load-displacement plots of the monotonic tests are presented in Fig. 4. The maximum loads attained were 2.90×10^4 N for

specimen CM8 with a displacement of 0.125 m at that load and a maximum load of 6.15×10^4 N for specimen TM8 with a corresponding maximum displacement of 0.265 m. These results showed that encasing a reinforced concrete member with a GFRP tube increased its resistance and its displacement at maximum load by 112%. It can also be seen in Fig. 4 that the load displacement curve of specimen CM8 flattened when the reinforcing steel

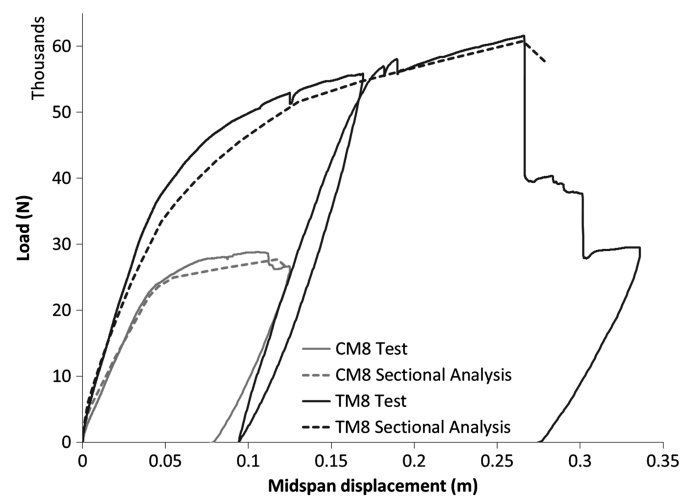


Fig. 4. Load deflection plots of monotonic tests and predictions

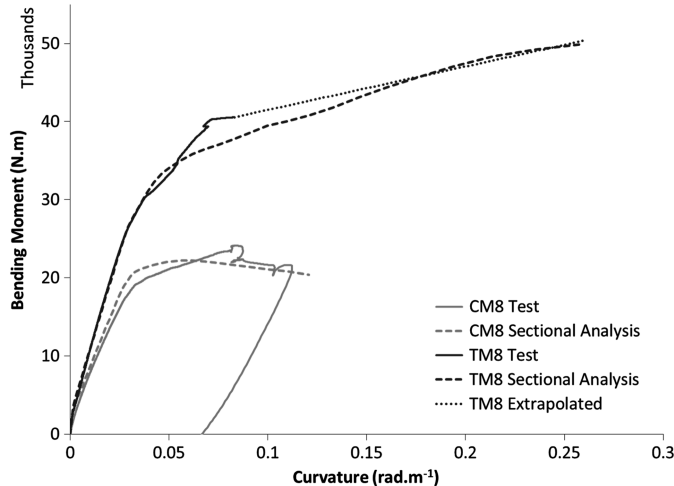
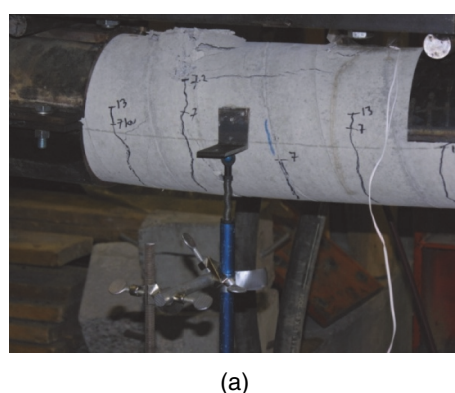


Fig. 5. Moment curvature plots of monotonic tests and predictions

yielded, while that of specimen TM8 continued to increase, although at a slower rate. This was attributed to the tube continuing to carry increasing loads in the case of specimen TM8. The areas under the load displacement curves at failure, corresponding to the total stored strain energies of the specimens, were 2.4 kJ for specimen CM8 and 14.1 kJ for specimen TM8. Thus, the addition of the GFRP tube increased specimen TM8's strain energy capacity by 488% when compared to specimen CM8. This increase represented a substantial potential increase in blast resistance. Additionally, Fig. 5 presents the experimental moment-curvature relationships of the monotonic specimens. The experimental curvature was calculated using the measured strains and the known rebar arrangement, assuming that plane sections remained plane. The strain gauges failed due to the large strains while testing specimen TM8, therefore, the final point on that moment-curvature plot was calculated using the maximum load and the peak displacement of the test.

Fig. 6(a) shows the failure mechanism of specimens CM8, and Fig. 6(b) shows the failure mechanism of specimen TM8. Specimen CM8 failed by crushing of the concrete in compression after yielding of the steel in tension, while specimen TM8 failed by rupture of the tube in tension after yielding of the steel in tension. As specimen TM8 attained a much higher load, it can be inferred that the tube protected the concrete and prevented it from crushing and spalling due to the confinement it exerted.



(a)

Table 3. Summary of Experimental Results

Specimen	Testing method	Type	Reinforcement ratio (%)	Residual displacement
CB4	50 kg of C4	RC	1.2	0.090 m
CB8-S	50 kg of C4	RC	2.4	0.035 m
CB8-L	100 kg of C4	RC	2.4	0.070 m
TB4	50 kg of C4	CFFT	1.2	0.020 m
TB8-S	50 kg of C4	CFFT	2.4	0.000 m
TB8-L	100 kg of C4	CFFT	2.4	0.050 m

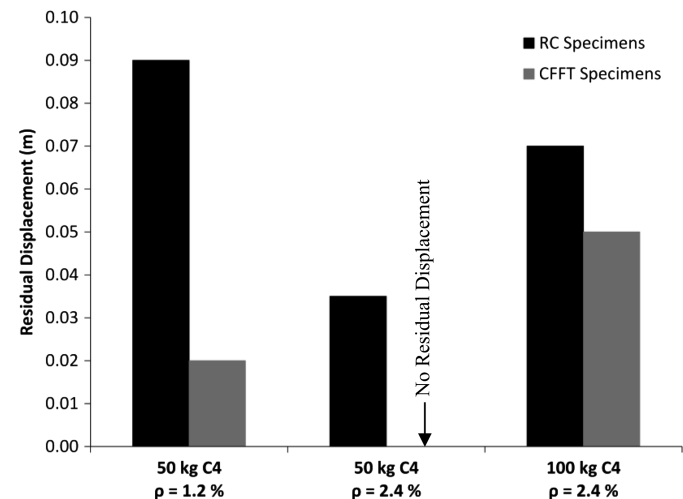


Fig. 7. Comparative residual displacements of monotonic and blast testing specimens

Damage and Residual Displacement of Blast Tests

The blasts did not inflict any visible damage to the GFRP tubes of the CFFT specimens in any of the tests in this study. All the reinforced concrete specimens, on the other hand, experienced crushing of the concrete on the compressive side. Specimen CB8-L also experienced spalling of concrete on the tensile side. Thus, the GFRP tube, in addition to withstanding the blast's shock wave, contained and protected the reinforced concrete core from localized damage. The addition of the GFRP tube also reduced the residual displacements in all the tests. This can be seen in Table 3 and Fig. 7 which present the residual displacements of the blast tested CFFT and reinforced concrete specimens. It can be clearly seen that the CFFT



(b)

Fig. 6. Failure mechanism of (a) specimens CM8; (b) specimen TM8

specimens consistently outperformed the reinforced concrete specimens.

Specimen CB4 had a 0.09 m residual displacement at midspan as well as significant concrete compression crushing when subjected to a blast from 50 kg of C4 as can be seen in Fig. 8(a). Specimen TB4, specimen CB4's counterpart, had a residual midspan displacement of 0.02 m and no visible damage to the tube. Specimen CB8-S had a residual midspan displacement of 0.035 m and the concrete in compression crushed as can be seen in Fig. 8(b). Specimen TB8-S, specimen CB8-S's counterpart, had no residual midspan displacement or any visible damage. Specimen CB8-L had a residual midspan displacement of 0.07 m and extensive crushing on the compression side and spalling on the tension side, as can be seen in Fig. 8(c). Specimen TB8-L, specimen CB8-L's counterpart, had a residual midspan displacement of 0.05 m and no visible breach of the tube. Thus, the addition of a GFRP tube reduced the residual displacement by 100% for a blast of 50 kg of C4 and 29% for a blast of 100 kg of C4. Doubling the reinforcement ratio from 1.2 to 2.4% decreased the residual displacement by 61% for the reinforced concrete specimens and 100% for the CFFT specimens for a blast of 50 kg of C4. Inspecting the values in Table 3 reveals that both specimen CB4 and CB8-L had residual displacements comparable to the residual displacement of specimen CM8 after unloading during the monotonic test.

This gives an estimate of the energy imparted to the specimens to be approximately in the range of 2–3 kJ.

Analysis of Test Results

Sectional Analysis of Monotonic Tests

A sectional analysis calculates a member's response by imposing strain compatibility between the concrete and the reinforcement, assuming that plane sections remain plane (Bentz 2000). The member's full response is calculated by satisfying equilibrium of the cross section's internal forces for incrementally increasing strain profiles. The resulting moments and curvatures are then calculated using these internal forces and strain profiles.

The member's constitutive material's stress-strain relationships need to be known in order to relate the member's deformation to the developed internal forces. The reinforced concrete specimens' concrete stress strain curve was modeled using the curve developed by Popovics (1973). The tube in the CFFT specimens, however, partially confined the concrete. Therefore, the CFFT specimens' concrete strength was held at the concrete's compressive strength once that value was reached to account for the resulting plastic behavior, as described by Cole and Fam (2006). These two concrete stress-strain curves are shown in Fig. 9. The stress-strain curves of the



Fig. 8. Damage to blast tested specimens

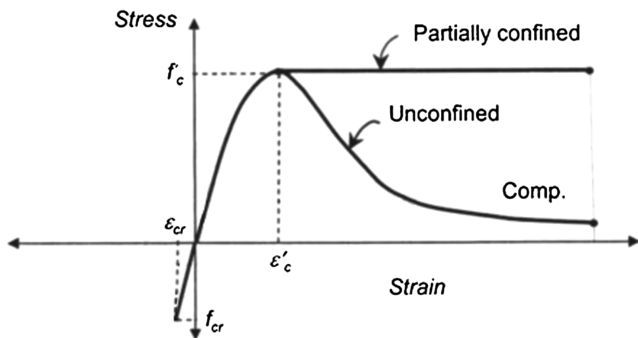


Fig. 9. Concrete stress-strain curves used in sectional analyses (adapted from Cole and Fam 2006, © ASCE)

longitudinal and transverse reinforcement, as well as that of a tube with comparable laminate structure tested by Zakaib (2013), are shown in Fig. 10. The tensile portion of the tube was modeled by idealizing the curve presented in Fig. 10 into an elastic-perfectly plastic curve. It was observed while reviewing the literature that tubes with similar laminate structures (Fam et al. 2005; Mandal 2004) behave more linearly under compression than under tension, probably as much of the nonlinearity is introduced by the splitting of the matrix between the fibers. Additionally, it was observed that in the cases previously mentioned, the stiffness under compression was 60% higher than that under tension. Due to these observations, the portion of the tube under compression was assumed to act linearly, and its stiffness was adjusted to match the experimental moment curvature results. This stiffness increase may have been caused by the lateral restraint provided by the concrete core, which was not present in the coupon tests referred to previously. The sectional analysis was terminated when the concrete crushed in the reinforced concrete specimens and when the tube ruptured in the CFFT specimens.

Sectional analysis predictions of the load-displacement and moment-curvature responses of the two monotonic specimens, CM8 and TM8, are presented in Figs. 4 and 5, respectively. The sectional analysis results matched the experimental results closely. Thus, the sectional analysis results for specimens CM8 and TM8 were used for specimens CB8, and TB8 as they had the same reinforcement arrangement. Similar sectional analyses were performed to obtain

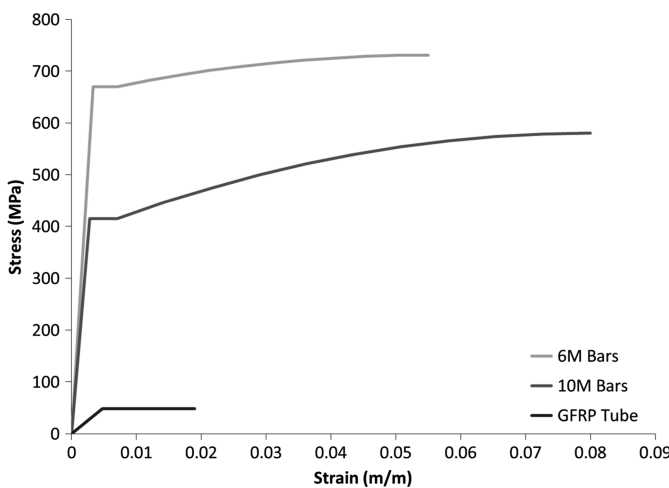


Fig. 10. Stress-strain curves of steel and GFRP tube used in sectional analyses

the equivalent monotonic moment-curvature relationships of specimens CB4 and TB4.

Close-In Blast Peak Force and Impulse

Suspending the charges on top of the specimens practically limited the type of loading to close-in blasts. This caused the pressure wave to be highly nonuniform and the blast parameters to vary significantly at different locations on the specimens at any point in time. Thus, the blast parameters obtained from the standard design charts did not accurately reflect the load experienced by the specimens. Additionally, the pressure wave reflected off of the ground and exerted an upward pressure on the specimens which reduced the effective imparted impulse. To overcome these difficulties, the commercially available hydrocode *ANSYS Autodyn* was used to develop a forcing function that was used to estimate the peak force and imparted impulse. The following sections will give the details of the procedure.

Model Description

A relatively simple model was utilized to obtain the forcing functions. The quarter symmetry model consisted of an Euler part to model the blast wave and its interaction with the structure. This was coupled to a rigid half-cylinder representing the specimen, which provided a boundary for the blast wave to diffract around. A set of three circumferential numerical gauges, one at the top, one at the side, and one at the bottom, were placed at 0.25 m intervals along the length of the cylinder to record the resulting pressure-time histories. The Euler part had dimensions of $0.7 \times 2.7 \times 2.0$ m and had outflow boundaries on all faces other than the planes of symmetry and the ground. The standard material models for Air and C4 that are built into the software were used in the simulation. The blast was modeled in one dimension from initiation until the shock-wave had almost reached the specimen, after which the results were remapped onto the 3D model using *Autodyn*'s built in remapping capabilities. The simplicity of the model allowed for the use of a fine 10 mm cubic mesh to capture the fine detail of the loading. The model, including the gauges and mesh, is shown in Fig. 11.

Forcing Function Derivation Procedure

The following procedure was adopted to develop the close-in blast forcing function from the highly non uniform pressure-time histories at the gauge point locations:

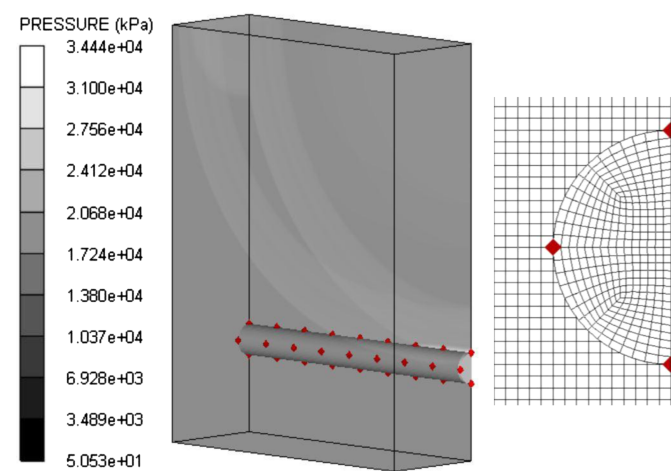


Fig. 11. Numerical model used to construct close-in test blasts forcing functions

- The ambient atmospheric pressure was subtracted from all pressure results;
- The equivalent downwards and upwards pressures acting on the specimen's circular cross section were obtained using Eq. (1), the development of which is reported elsewhere (Qasrawi et al. 2010)

$$P_{eq} = \frac{2}{3\pi}[2P_r + P_{so}] \quad (1)$$

where P_{eq} = equivalent effective pressure; P_r = reflected pressure; and P_{so} = side-on pressure;

- Equivalent upward and downward point loads were then obtained by multiplying the obtained pressures by the gauge points' tributary area on the specimen's surface. This surface area corresponded to half the circumference multiplied by the distance between the gauges (The distance used was 0.25 m except for the end gauge where 0.125 m was used); and
- The equivalent upward and downward forces were then summed at each gauge location at each time increment as described in Unified Facilities Criteria (UFC 3-340-01 2002) for impulsive loads and multiplied by 2 to account for symmetry.

The resulting forcing functions and impulses are presented in Fig. 12. The maximum force and impulse for the two charges were 3.1×10^6 N and $376.4 \text{ N} \cdot \text{s}$ for the 50 kg of C4 charge, and 4.7×10^6 N and $845.7 \text{ N} \cdot \text{s}$ for the 100 kg of C4 charge. The forces were divided by half the surface area of the specimen to convert them to pressures. The impulse time unit was also converted to milliseconds. The obtained pressure and specific impulse values were 2.42 MPa and 0.287 MPa · ms for the 50 kg C4 charge and 3.59 MPa and 0.644 MPa · ms for the 100 kg charge C4.

Single Degree of Freedom Modeling

A single degree of freedom (SDOF) system is one whose complete motion can be described using one coordinate.

The analysis of flexural members can be simplified to an SDOF by assuming a shape function that is scaled by a single displacement of interest, usually the midspan displacement. The equivalent mass, stiffness, and forcing function can be obtained by equating the kinetic, strain, and potential energies of the SDOF system to the original system. These SDOF properties can then be used to construct Pressure-Impulse diagrams to aid in blast resistant design.

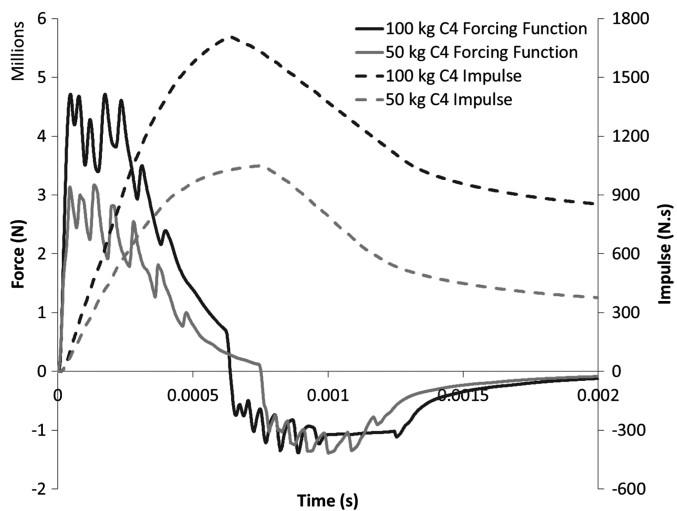


Fig. 12. Derived blast test forcing and impulse time histories

Equivalent Mass (M_{eq})

An SDOF system has a lumped equivalent mass that undergoes rigid body motion. The modeled specimens, however, had a distributed mass that underwent different accelerations at different locations along the span. The close-in nature of the blast meant that the loading dispersed before the specimens had time to respond significantly. Consequently, the majority of the motion of the specimens occurred under free vibration, the shape function of which is sinusoidal. Thus, the equivalent masses were calculated by assuming a sinusoidal deformed shape and equating the kinetic energies of the two systems. The calculated equivalent masses, the total masses, and the distributed masses of the blast specimens given in Table 4.

Resistance Functions

Resistance functions were derived for the experimental specimens by equating the work done by applied forces to work done by an equivalent force applied at midspan. This was achieved for a given cross section and loading arrangement as follows: A moment-curvature relationship was obtained from a sectional analysis for the investigated cross section. The loading was assumed to be a sinusoidally distributed load for the blast specimens as the impulsive blast shockwave dissipated before the specimens deformed substantially and the resulting oscillations were free vibrations. A bending moment diagram was constructed for a load increment applied to the specimen in the same arrangement as the external load. The bending moment diagram and the moment-curvature relationship were used to find the curvature distribution along the length for the load increment. This curvature distribution along the length was used to calculate the displacement using the double integration method. The moment-curvature relationship was also integrated with respect to curvature to give a relationship between the strain energy and curvature. This strain energy-curvature relationship was used with the curvature distribution along the length to find the strain energy distribution along the length of the specimen for the load increment. This strain energy distribution was then integrated to find the total strain energy for the load increment. Increasing the load increment and repeating this procedure resulted in the total strain energy as a function of displacement. The numerical derivative of this strain energy-displacement function was taken with respect to displacement to obtain the resistance function.

The sectional moment-curvature relationships for the specimens were increased by a dynamic increase factor (DIF) to account for enhancements in material properties due to high strain rates (UFC 3-340-01 2002). The DIFs were calculated using strain rates measured during impact testing reported elsewhere (Qasrawi 2014). The impact testings' DIFs were assumed adequate because of the minimal damage to the blast-tested CFFT specimens indicating that the maximum displacements attained were small. As the periods are similar for the blast and impact tested specimens, the time to reach the maximum displacements were also similar, which in turn meant that the strain rates were similar. The moment-curvature curves are presented in Fig. 13. The resulting

Table 4. Total and Equivalent Specimen Masses

Specimen designation	Total mass (kg)	Distributed mass (kg/m)	Equivalent SDOF mass (kg)	Mass factor K_M
CB4	357	89.3	171.6	0.481
TB4	383	95.8	184.1	0.481
CB8	370	92.5	177.9	0.481
TB8	396	99.0	190.4	0.481

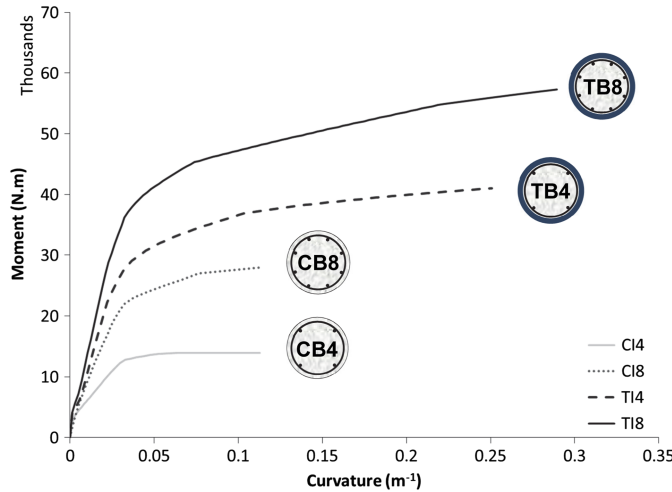


Fig. 13. Moment-curvature of blast specimens, including DIF

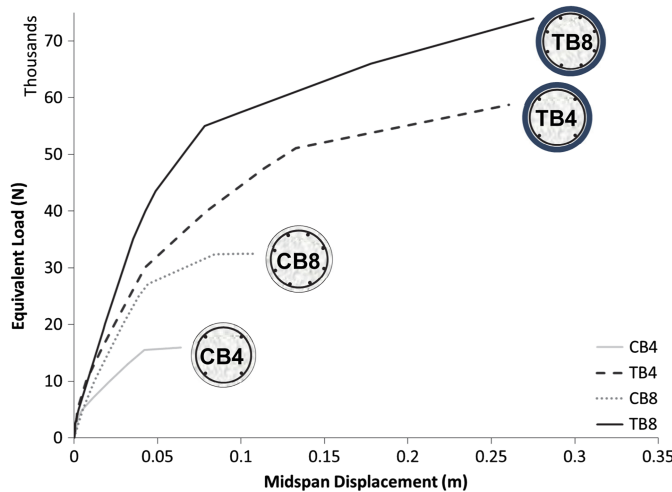


Fig. 14. Blast tested specimens' resistance functions

resistance functions derived in this way for the blast testing specimens are presented in Fig. 14.

Pressure Impulse diagrams

In general, a transient load applied to a structure can fall in one of three categories or regimes. The first is the impulsive regime where the load dissipates before the structure has responded significantly. In this case, the energy of the load is assumed to be transformed into kinetic energy in the structure by imparting an initial velocity. This regime is considered a response limit, as the behavior is not affected by the peak force due to the short duration of the load. To calculate this limit of response, all of the specimen's initial kinetic energy is assumed to be converted into strain energy. Thus the impulse can be calculated for a SDOF system using Eq. (2) as follows:

$$I = \sqrt{2M_{eq} \int_0^{y_{max}} R(y) dy} \quad (2)$$

where I = impulse; M_{eq} = SDOF equivalent mass; y_{max} = SDOF displacement of interest; and $R(y)$ = SDOF resistance function.

The other response limit, known as quasi-static loading, is where the structure has fully responded before the load has dissipated significantly. In this case the behavior is determined by the peak force rather than the impulse. It is assumed that all the work done by the applied force is converted to strain energy in the structure and the force can be calculated using Eq. (3)

$$F = \frac{\int_0^{y_{max}} R(y) dy}{y_{max}} \quad (3)$$

where F = force; y_{max} = SDOF displacement of interest; and $R(y)$ = SDOF resistance function.

In both these regimes, the response of the structure can be assumed to be independent of the load time history and to only depend on the impulse in the first case and the maximum force in the second.

In the third, or dynamic, regime, the load and the structure interact and a full dynamic analysis is necessary to predict the response. The hyperbolic formula given in Eq. (4), adapted from (Krauthammer 2008), was used to approximate this dynamic region

$$S.E. = W.D. \tanh^2 \sqrt{(K.E./W.E.)} \quad (4)$$

where S.E. = strain energy; W.D. = work done; and K.E. = kinetic energy.

Eq. (4) can be rewritten as Eq. (5) using Eqs. (2) and (3) as follows:

$$\int_0^{y_{max}} R(y) dy = F y_{max} \tanh^2 \sqrt{\frac{I^2}{2M_{eq} F y_{max}}} \quad (5)$$

Eq. (5) can be solved numerically in the dynamic region by assuming a value for the impulse for a given strain energy and iteratively solving for the corresponding maximum force.

According to Hansen (Hansen et al. 2006), the US Army Corps of Engineers proposes the following component response limits for design: A maximum support rotation of 0.52° to indicate light damage, a maximum support rotation of 2.94° to indicate moderate damage, and a maximum support rotation of 6.67° to indicate heavy damage. The midspan displacements, for the span length investigated in this study, corresponding to these limits are 0.018, 0.099, and 0.225 m, respectively.

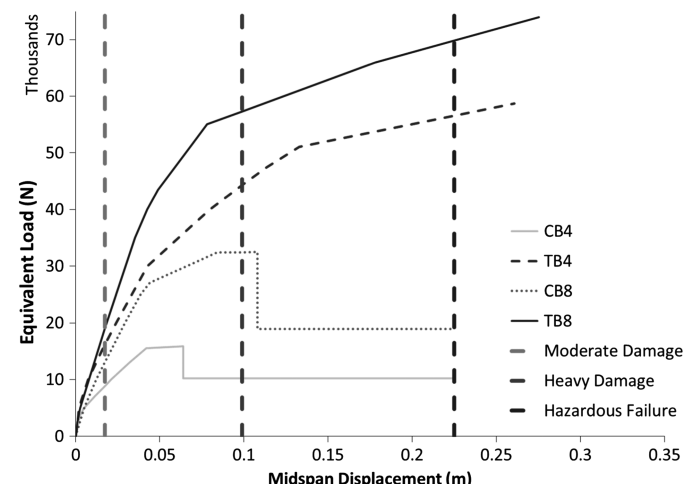


Fig. 15. Extended resistance functions and blast design limits

Table 5. Pressure Impulse Diagrams' Asymptotes for Blast Tested Specimens

Specimen designation	Y_{\max} (m)	Strain energy (J)	Force (N)	Impulse (N.s)	Pressure (MPa)	Specific impulse (MPa · ms)
CB4	0.018	102	5,667	187	0.0043	0.142
	0.099	1,110	11,200	616	0.0085	0.467
	0.225	2,400	10,700	907	0.0081	0.687
CB8	0.018	127	7,060	213	0.0053	0.161
	0.099	2,350	23,700	914	0.0180	0.693
	0.225	4,860	21,600	1,310	0.0164	0.996
TB4	0.018	179	9,944	257	0.0075	0.195
	0.099	2,870	29,010	1,030	0.0220	0.779
	0.225	9,460	42,022	1,870	0.0318	1.410
TB8	0.018	186	10,300	266	0.0078	0.202
	0.099	3,810	38,500	1,200	0.0292	0.913
	0.225	11,900	52,800	2,130	0.0400	1.610

It is assumed that the concrete in the heavy damage criteria above is significantly damaged and its contribution to resistance is typically ignored. To account for this the UFC 3-340-01 (UFC 2002) divides reinforced concrete sections into two types based on their response. In the Type I cross section, the compressive concrete is intact and contributes to the moment resistance with the reinforcing steel. In the Type II cross section, on the other hand, the concrete is assumed to have been crushed completely and the steel reinforcement resists all the applied loads. Thus the Type II cross section's moment capacity is calculated using Eqs. (6) and (7)

$$M_p = \sum_{i=1}^n F_i d_i \quad (6)$$

$$F = \text{DIF}(F_{ds}A) \quad (7)$$

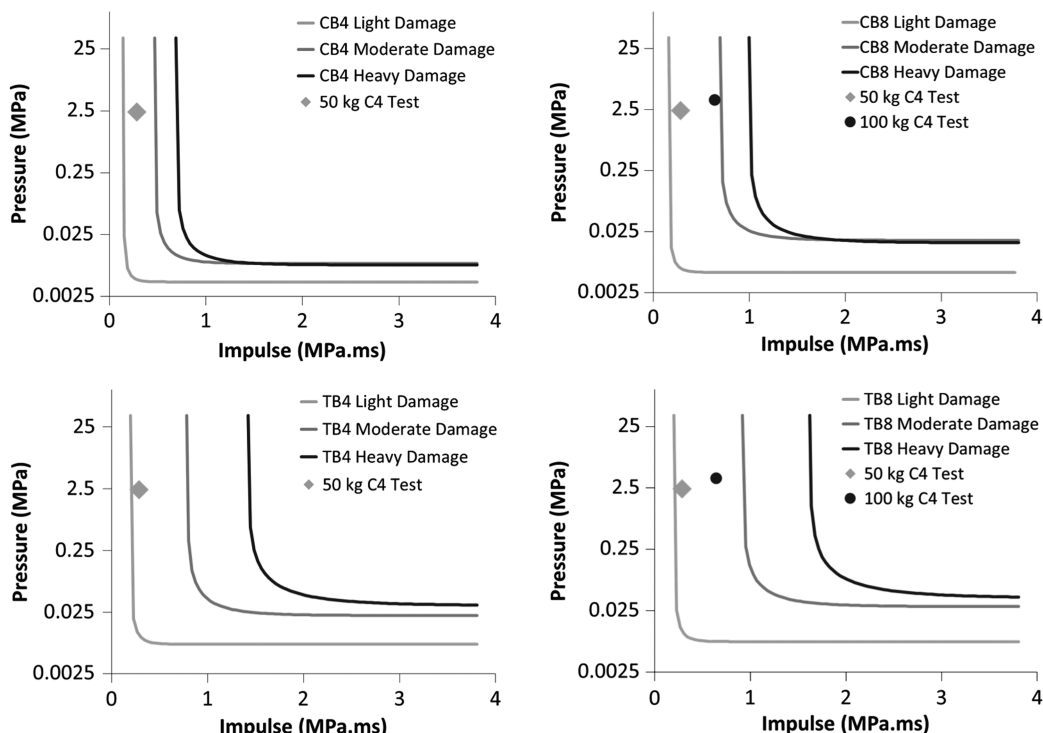


Fig. 16. Pressure impulse diagrams of blast tested specimens

where M_p = plastic moment resistance; F_i = force in the reinforcement layer i ; d_i = lever arm to reinforcement layer i ; DIF = dynamic increase factor; A = reinforcement layer's cross-sectional area; and

F_{ds} = steel reinforcement's dynamic stress, taken to be the yield stress for members with a length to depth ratio larger than 10 [Table 10-2 of the UFC 3-340-01 (UFC 2002)].

The Type II section's equivalent resistance is calculated from the moment capacity using Eq. (8), which was derived assuming that the beam is undergoing free vibration and that a plastic hinge has formed at midspan

$$R_u = \frac{4M_p}{L} \quad (8)$$

Therefore, the Type II section moment capacity of specimen CB4 was 9864 N · m and that of specimen CB8 was 18216 N · m. These moment capacities translated to resistances of 10248 and 18925 N for specimens CB4 and CB8, respectively. The derived resistance functions for specimens TB4 and TB8 extended past the design limit of 0.225 m, therefore, the preceding calculation was unnecessary for them. The extended resistance functions and the blast design limits are presented in Fig. 15. The calculated impulse, force, strain energy, pressure, and specific impulse for all the specimens for the blast design limits are presented in Table 5. The peak pressure and specific impulse were obtained from the force and impulse by dividing by half the cylindrical surface area of the specimens. The pressure-specific impulse diagrams are presented in Fig. 16 for all specimens.

Plotting the previously derived peak pressure and impulse of the test blasts on the Pressure-Impulse diagrams in Fig. 16 shows clearly that the tests were highly impulsive as expected. The experimental blasts fell below the moderate damage limit for all the specimens, a result that is supported by the experimental observations. Specimens' CB4, CB8-S, and CB8-L strength were overestimated.

This was attributed to the observed spalling in these specimens which must have occurred early (UFC 3-340-01 2002) in the response and changed the resistance and response of the members as well as the effect of the mirror boundary in the blast loading model. The heavy damage curve of specimens CB4 and CB8 falls below the moderate damage curve. This was due to the significant reduction in strength when a Type II section develops, causing the force calculated by equating the work done to the strain energy to be lower than that for the moderate damage case.

The results presented so far have not included an axial load, which would imply that these results are limited to flexural members. Axial loads, however, can be easily incorporated into the analysis by including them in the force equilibrium of the sectional analysis when calculating the moment-curvature relationship. The following points need to be investigated before the procedure is extended with confidence. First, whether the axial load remains constant or varies as the member deforms. Second, quantifying the second order effects resulting from the axial load.

The procedure outlined in this section can be used to derive close-in blast loads and P-I diagrams relatively easily for any cross-section and lends itself to blast resistant analysis and design. The observations made in this investigation imply that the simply supported reinforced concrete member recommended end rotations may be too conservative for the CFFT system as the tube confines and protects the concrete, allowing the member to undergo much larger displacements.

Conclusions

The results of the monotonic tests carried out in this study have shown that the addition of a GFRP tube to a reinforced concrete member increased the monotonic load carrying capacity and displacement at maximum load by 112% as well as increasing its monotonic energy absorbing capacity by a factor of 488%, primarily due to concrete confinement. This has motivated launching experimental and analytical investigations into the dynamic response of these members under blast loading with the promise of excellent response and energy absorption due to the addition of the GFRP tube.

While all the reinforced concrete specimens in this study experienced concrete damage under blast loading, none of the tubes of the CFFT specimens were breached. The addition of a GFRP tube eliminated the residual displacement for a blast of 50 kg of C4 and reduced it by 29% for the CFFT specimens and a blast of 100 kg of C4 when compared to the control reinforced concrete counterpart. Doubling the reinforcement ratio from 1.2 to 2.4% eliminated the residual displacement of the CFFT specimens for a blast of 50 kg of C4. This indicates that encasing reinforced concrete members with GFRP tubes is desirable for enhanced blast resistance. These results were anticipated based on the monotonic and sectional analysis results, however, the additional benefit of protecting and containing the concrete core only became apparent after blast testing.

Numerical procedures for developing close-in blast forcing functions, nonlinear resistance functions, and pressure-impulse diagrams for CFTTs for use in blast resistant analysis and design were presented and compared well to experimental results. The Pressure-Impulse diagrams were constructed for the experimental specimens, which agreed well with the experimental test blasts.

The procedures outlined in this chapter for developing equivalent close-in blast forcing functions and Pressure-Impulse diagrams will greatly assist in the practical task of designing structural

members to resist close in blasts. This should help produce more robust structures and members, which can in turn save lives and property.

References

- Ameron International. (1988). *Series 5000 fiberglass pipe and fittings: For severely corrosive industrial service*, Bondstrand Product Data, Houston.
- ANSYS Autodyn [Computer software]. Canonsburg, PA, x64 Academic Research.
- Bentz, E. (2000). *Sectional analysis of reinforced concrete members*, Ph.D. thesis, Univ. of Toronto, Toronto, ON, Canada.
- Buchan, P. A., and Chen, J. F. (2007). "Blast resistance of FRP composites and polymer strengthened concrete and masonry structures—A state-of-the-art review." *Composites Part B*, 38(5–6), 509–522.
- Canadian Standards Association (CSA). (2004a). "Compressive strength of cylindrical concrete specimens." A23.2-9C, Mississauga, ON, Canada.
- Cole, B., and Fam, A. (2006). "Flexural load testing of concrete-filled FRP tubes with longitudinal steel and FRP rebar." *ASCE J. Compos. Constr.*, 10.1061/(ASCE)1090-0268(2006)10:2(161), 161–171.
- Crawford, J. E. (2013). "State of the art for enhancing the blast resistance of RC columns with FRP." *Can. J. Civ. Eng.*, 40(11), 1023–1033.
- Elgawady, M., Booker, A., and Dawood, H. (2010). "Seismic behavior of posttensioned concrete-filled fiber tubes." *ASCE J. Compos. Constr.*, 10.1061/(ASCE)CC.1943-5614.0000107, 616–628.
- Fam, A., and Mandal, S. (2006). "Prestressed concrete-filled fiber-reinforced polymer circular tubes tested in flexure." *PCI J.*, 51(4), 42–54.
- Fam, A., and Rizkalla, S. (2002). "Flexural behavior of concrete-filled fiber-reinforced polymer circular tubes." *ASCE J. Compos. Constr.*, 10.1061/(ASCE)1090-0268(2002)6:2(123), 123–132.
- Fam, A., Schnerrich, D., and Rizkalla, S. (2005). "Rectangular filament-wound glass fiber reinforced polymer tubes filled with concrete under flexural and axial loading: Experimental investigation." *ASCE J. Compos. Constr.*, 10.1061/(ASCE)1090-0268(2005)9:1(25), 25–33.
- Flisak, B., Fam, A. Z., and Rizkalla, S. H. (2001). "FRP tubes filled with concrete and subjected to combined axial and flexural loads." *Proc., Construction Institute Sessions at the ASCE Civil Eng.*, 45–54.
- Fujikura, S., Bruneau, M., and Lopez-Garcia, D. (2008). "Experimental investigation of multihazard resistant bridge piers having concrete-filled steel tube under blast loading." *J. Bridge Eng.*, 10.1061/(ASCE)1084-0702(2008)13:6(586), 586–594.
- Hansen, E., Levine, H., Lawver, D., and Tennant, D. (2006). "Computational failure analysis of reinforced concrete structures subjected to blast loading." *Proc., 17th Analysis and Computation Specialty Conf.*, ASCE, St. Louis, MO.
- Helmi, K., Fam, A., and Mufti, A. (2008). "Fatigue life assessment and static testing of structural GFRP tubes based on coupon tests." *ASCE J. Compos. Constr.*, 10.1061/(ASCE)1090-0268(2008)12:2(212), 212–223.
- Krauthammer, T. (2008). *Modern protective structures*, CRC Press, Boca Raton, FL.
- Malvar, L. J., Crawford, J. E., and Morrill, K. B. (2007). "Use of composites to resist blast." *ASCE J. Compos. Constr.*, 10.1061/(ASCE)1090-0268(2007)11:6(601), 601–610.
- Mandal, S. K. (2004). *Prestressed concrete-filled fiber reinforced polymer tubes*, Master's thesis, Queen's Univ., Kingston, ON, Canada.
- Popovics, S. (1973). "A numerical approach to the complete stress-strain curve of concrete." *Cem. Concr. Res.*, 3(5), 583–599.
- Qasrawi, Y. (2014). "The dynamic response of concrete filled FRP tubes subjected to blast and impact loading." Ph.D. thesis, Queen's Univ., Kingston, ON, Canada.
- Qasrawi, Y., and Fam, A. (2008). "Flexural load tests on new spin-cast concrete-filled fiber-reinforced polymer tubular poles." *ACI Struct. J.*, 105(6), 750–759.

- Qasrawi, Y., Heffernan, P., and Fam, A. (2010). "Numerical determination of reflected blast pressure distribution on round columns." *Proc., Conf. Structures under Shock and Impact XI*, Tallinn, Estonia, 83–92.
- Unified Facilities Criteria. (2002). "Design and analysis of hardened structures to conventional weapons effects." *UFC 3-340-01*, Dept. of Defense, Washington, DC.
- Zaghi, A. E., Saiidi, M. S., and Mirmiran, A. (2012). "Shake table response and analysis of a concrete-filled FRP tube bridge column." *Compos. Struct.*, **94**(5), 1564–1574.
- Zakaib, S. E. (2013). "Flexural performance and moment connections of concrete-filled GFRP tubes (CFFTS) and CFFT-encased steel I-sections." Master's thesis, Queen's Univ., Kingston, ON, Canada.